ARTICLE

# Resistance of Nanoclay Reinforced Epoxy Composites to Hyperthermal Atomic Oxygen Attack

Hei-long Wang[a,b], Vanessa J. Murray[c], Min Qian[d], Donna J. Minton[c], Ai-yi Dong[a], Kin-tak Lau[e], Bo-han Wu[f], Li Che[a*], Timothy K. Minton[c*]

*a. College of Science, Dalian Maritime University, Dalian 116026, China*
*b. State Key Laboratory of Molecular Reaction Dynamics, Dalian Institute of Chemical Physics, Chinese Academy of Sciences, Dalian 116023, China*
*c. Department of Chemistry and Biochemistry, Montana State University, 103 Chemistry and Biochemistry Bldg., Bozeman, Montana 59717, United States of America*
*d. Department of Physics, School of Science, East China University of Science and Technology, Shanghai 200237, China*
*e. Faculty of Science, Engineering and Technology, Swinburne University of Technology, Hawthorn VIC 3122, Australia*
*f. Beijing Institute of Spacecraft Environment Engineering, Beijing 100094, China*

(Dated: Received on June 20, 2019; Accepted on September 12, 2019)

Due to outstanding mechanical properties, heat resistance, and relatively facile production, nanoclay reinforced epoxy composites (NCRE composites) have been suggested as candidate materials for use on external surfaces of spacecraft residing in the low Earth orbit (LEO) environment. The resistance of the NCRE composites to bombardment by atomic oxygen (AO), a dominant component of the LEO environment, has been investigated. Four types of samples were used in this study. They were pure epoxy (0 wt% nanoclay content), and NCRE composites with different loadings of nanoclay—1 wt%, 2 wt%, and 4 wt%. Etch depths decreased with increasing nanoclay content, and for the 4 wt% samples it ranged from 28% to 37% compared to that of pure epoxy. X-ray photoelectron spectroscopy (XPS) indicates that after AO bombardment, relative area of C−C/C−H peak decreased, while the area of the C−O, ketones peaks increased, and the oxidation degree of surfaces increased. New carbon-related component carbonates were detected on nanoclay containing composite surfaces. Scanning electron microscopy indicates that aggregates formed on nanoclay-containing surfaces after AO bombardment. The sizes and densities of aggregates increased with nanoclay content. The combined erosion depths, XPS and SEM results indicate that although all the studied surfaces got eroded and oxidized after AO bombardment, the nanoclay containing composites showed better AO resistance compared to pure epoxy, because the produced aggregates on surface potentially act as a physical "shield", effectively retarding parts of the surface from further AO etching.

**Key words:** Atomic oxygen, Epoxy, Nanoclay, Low Earth orbit

## I. INTRODUCTION

While polymers could feasibly be important materials for use on the outer surfaces of spacecraft in low Earth orbit (LEO) [1, 2], the harsh environment of atomic oxygen (AO), ultraviolet (UV) and vacuum ultraviolet (VUV) radiation, extreme thermal fluctuations, space debris, ionizing radiation, and high vacuum, presents very challenging conditions for polymers. Polymeric materials flowed in the LEO environment have been shown to succumb to accelerated surface erosion and cracking, oxidation, material degradation, surface out gassing, and contamination [3−5]. For polymers, AO is arguably the most destructive one of these environmental hazards due to its relatively high concentration and powerful capacity for oxidation. The neutral atmosphere at 300 km altitude consists of ∼90% AO, with the remaining atmosphere containing $N_2$, He, $O_2$, $H_2$ and Ar. As spacecraft travels at orbital velocities of ∼8 km/s, the spacecraft surfaces collide with residual AO at high translational energies, up to 4−5 eV, and at nominal AO fluxes of $\sim 10^{14}$ to $10^{15}$ atom·cm$^{-2}$·s$^{-1}$ [6−8]. These conditions could easily lead to oxidation of exposed polymeric materials unless the material can be in some way protected from the highly energetic impinging AO.

Two possible ways of protecting polymeric materials

*Authors to whom correspondence should be addressed. E-mail: liche@dlmu.edu.cn, tminton@montana.edu

 

against AO erosion have been used, including coatings on the surfaces of exposed polymers and copolymerization or blending of an inorganic component to the polymer. Coatings typically consist of inorganic materials that can act as a protective layer, shielding the polymer from exposure to AO. Atomic layer deposition (ALD) of a ∼35 Å-thick $Al_2O_3$ film coated on Kapton-H showed negligible mass loss during exposure to beam of AO with a fluence of $1.2\times10^{20}$ atom/cm$^2$ [9]. Another study on a 100−300 nm-thick $TiO_2$ thin film coating made by liquid phase deposition resulted in a mass loss ratio of only 1%−2% compared to a Kapton-H reference sample after exposure to a beam of AO with a fluence of $1\times10^{20}$ atom/cm$^2$ [10]. While both of these studies display the effectiveness of coatings as a form of protection of polymers from AO erosion, such coatings can be easily compromised during flight from cracks caused by thermal cycling and/or damaging of the coating from collisions with space debris. Such events are not reversible and will leave the underlying polymer vulnerable to AO oxidation and erosion for the remainder of the mission.

Like coatings, the addition of an inorganic component to a polymer by copolymerization or blending can also reduce the inherent reactivity of the material, while at the same time having the additional benefit of being less susceptible to permanent damage by cracking and debris impacts. Unlike coatings, the inorganic component in copolymer or blend can conceivably be uniformly distributed within the polymer, effectively forming an inorganic oxide protective layer upon AO exposure that can be resistant against further AO attack while also having the ability to potentially "self-heal" if damaged during flight. Copolymerization of a polyimide matrix (which has the same chemical structure with Kapton-H) with polyhedral oligomeric silsesquioxane (POSS) or siloxane has shown promising resistance against AO exposure [11, 12]. Depending on the weight percentage of the POSS cage, the erosion yield of the POSS polyimides may be as little as ∼1% that of the Kapton-H based on the laboratory and space-flight experiments [12]. The reduced erosion yield in both exposures was attributed to protection of the underlying polyimide by a silica passivation layer that was formed on the surface upon exposure to AO [11].

While copolymerization can undoubtedly be an effective approach to increasing resistance of polymer materials to AO, production of these materials is complicated and costly. What's more, the optical property of polymer might be changed by copolymerization of higher content reinforcement materials. As a less costly and simpler approach, addition of nanoclay particles to polymers has recently been introduced as a way to enhance polymer performance [13−15]. Nanoclay powder is mainly composed of O and Si particles (containing small amounts of C, Al, Mg, Na, and N) that are 20−200 nm in size [16−18]. Nanoclay reinforcement, in the range of 1 wt%−4 wt%, in polymers has been shown to improve the mechanical and thermal performance of polymers [14, 19−21]. The addition of nanoclay to polymers has also been shown to increase resistance to an AO plasma. Upon exposure to AO plasmas, nanoclay reinforced epoxy (NCRE) produced via the Quickstep process and nanoclay reinforced melt extruded nylon 6 showed surface erosion thickness can be significantly reduced after the passivation silica layer was formed [22].

While the resistance of the nanoclay reinforced polymers (NCRPs) to oxidation shows promise in a plasma environment, their durability in the space environment has not been assessed. In order to understand the susceptibility of NCRPs to hyperthermal AO in the LEO environment, we exposed NCRE composites to a directed beam of ∼5 eV AO, which effectively replicates the AO exposure conditions experienced by materials in LEO [12]. The NCRE samples were prepared to ensure homogeneous nanoparticles distribution throughout the polymer matrix [15, 23]. The polymer chosen for study was epoxy because of its known uses for spacecraft in LEO [24−26]. Another important consideration is the high reactivity of epoxy in LEO [27]. So, while nanoclay could in principle be blended with many polymers, its ability to significantly reduce the reactivity of epoxy would be a true demonstration of its effectiveness. NCRE composites with different loadings of nanoclay—0 wt%, 1 wt%, 2 wt%, and 4 wt%—were exposed to beams of directed hyperthermal AO, at three different O-atom fluences, $3.82\times10^{20}$, $5.46\times10^{20}$, and $6.31\times10^{20}$ atoms/cm$^2$. Post-exposure etch depths were measured to estimate the erosion degree of NCRE samples. Surface morphology by SEM and surface chemistry by XPS analyses were completed both pre- and post-exposure to allow additional insight into the efficacy of the process by which the added nanoclay protects the epoxy from AO attack.

## II. EXPERIMENTS

### A. Preparation of nanoclay reinforced epoxy composites

The NCRE composites were synthesized by using the method we developed [15, 23]. Epoxy resin, Araldite GY 251 (Diglycidylether of bisphenol A, DGEBA), and hardener HY 956 (Triethylenetetramine) from CIBA-GEIGY, were used in the ratio of 5:1 by weight to form the base polymer materials [19]. Nanoclay particles, $SiO_2$, and DK4 series, from Zhejiang FengHong Clay Chemical Company, Ltd. China, were added into the base polymer materials to form NCRE composites. The mean diameter of the nanoclay particles was 25 nm, the apparent density was 0.35 g/cm$^3$, and the moisture content was less than 3%.

A detailed description of the NCRE preparation has been described elsewhere [15]. Briefly, the predetermined weight content of nanoclay was added into the epoxy resin. The nanoclay/epoxy resin was put into a

DOI:10.1063/1674-0068/cjcp1906119 

bell jar on a rotating platform under vacuum for 55 min to extract gas bubbles. In order to ensure the nanoclay to be as uniformly dispersed as possible, the following process was repeated for 5 min: rotating the platform from 0 to 930 r/min for 2 s, rotating the platform from 930 r/min to 0 r/min for 1 s, and allowing the mixture to rest on a stationary platform for 7 s. The hardener was then added, and the new mixture underwent the same spinning and resting process as described above for 1 h under vacuum until the viscosity increased to avoid any movement of nanoclay inside the resin and the semi-cured uniformly-dispersed nanoclay/epoxy sample. The semi-cured sample was then removed from the bell jar and stored in a vacuum chamber for 12 h at 40 °C to form the cured sample.

Four types of sample with different loadings of nanoclay were prepared in this study: pure epoxy (0 wt% nanoclay content), NCRE composites with 1 wt%, 2 wt%, and 4 wt% nanoclay content.

### B. Hyperthermal AO exposures

AO exposures of the NCRE samples were conducted using a hyperthermal laser-detonation source of atomic oxygen [28]. Details on the functioning of the source have been described elsewhere [29]. In these exposures, pulses of pure oxygen gas (99.9%) with a backing pressure of 550 psi, were introduced into the source nozzle through a pulsed valve. 200 μs after the pulsed valve was triggered, a pulse of 10.6 μm light (7.5 J/pulse) from a $CO_2$ laser was focused into the nozzle apex using a gold-coated mirror mounted 50 cm from the nozzle. Upon reaching the pulse of oxygen gas, the laser pulse initiated a breakdown of the molecular oxygen to AO and resulted in a ∼8 km/s beam of mostly neutral AO with some residual $O_2$ [29]. During the exposures, the center of the hyperthermal $O/O_2$ beam was directed into a triply differentially pumped mass spectrometer detector and the ratio and velocity distributions of O and $O_2$ in the beam were collected, allowing for exact velocity distributions of the AO beam for each exposure to be ascertained. For the exposures described herein, the hyperthermal $O/O_2$ beams ranged from 88% to 95% neutral O atoms, 5%−12% $O_2$ molecules, and <0.01% ions.

Samples were placed in a sample mount located at 40 cm from the apex of the conical nozzle and were exposed to beams of hyperthermal $O/O_2$ with three different fluence: $3.82\times10^{20}$, $5.46\times10^{20}$, and $6.31\times10^{20}$ atom/cm$^2$. Translational energy distributions of hyperthermal $O/O_2$ beams were determined from the time-of-flight (TOF) distributions collected for the beams (FIG. 1). The $3.82\times10^{20}$ and $5.46\times10^{20}$ atom/cm$^2$ AO exposures, performed at the Dalian Institute of Chemical Physics, had a beam translational energy of 4.5 eV and full width of half maximum (FWHM) of 2.2 eV. The $6.31\times10^{20}$ atom/cm$^2$ AO exposure, performed at Montana State University had a beam translational energy of 5.3 eV and FWHM of 1.8 eV.

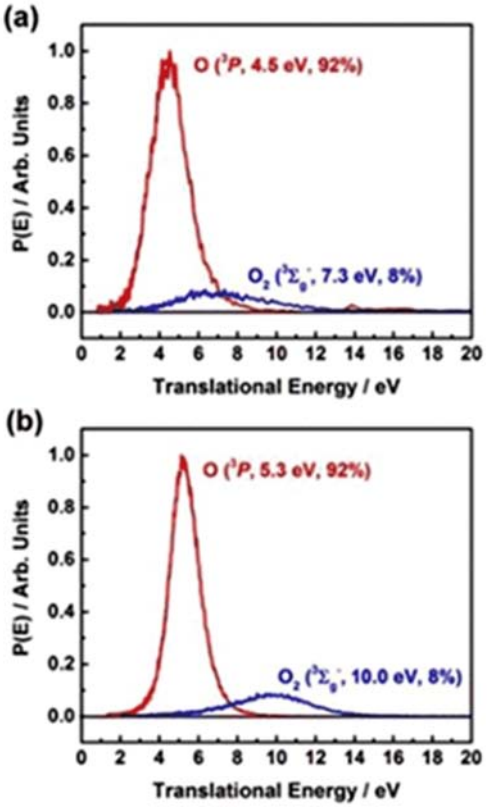


FIG. 1 Translational energy distributions of hyperthermal $O/O_2$ beams for (a) $3.82\times10^{20}$ and $5.46\times10^{20}$ atom/cm$^2$, (b) $6.31\times10^{20}$ atom/cm$^2$ AO exposures.

All samples (∼5 mm×15 mm×18 mm) were mounted on the sample holder by using double sided carbon conductive tape at room temperature (25 °C) during all exposures. In order to get the etch depth, all the NCRE composites were partially covered by Kapton-H strips (∼2 mm×15 mm), with 2 mm wide gaps between each other, which is shown in FIG. 2 (upper right and lower right) taking pure epoxy as an example. In this way, during the AO exposure process the area not covered by the Kapton-H strips was exposed to AO, yet the area covered was not, which makes the edge between exposed and unexposed area form a step and etch depth can be measured. Kapton-H reference samples were also mounted on the sample holder in order to obtain AO fluence and estimate for the three exposure conditions, which is shown in FIG. 2 (upper left and lower left). Kapton-H reference sample was covered with a stainless steel mesh disc (about 10 mm diameter, 100 μm thick) in order to form a step between exposed and unexposed areas during exposure, which was used to estimate the AO fluence.

DOI:10.1063/1674-0068/cjcp1906119 

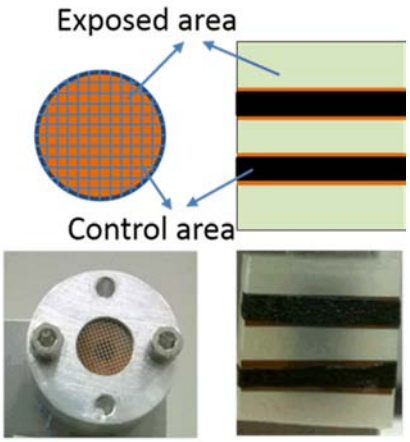


FIG. 2 The schematic diagram (upper) and photograph (lower) of sample holding method. Left panels: Kapton-H sample. Right panels: pure epoxy samples.

### C. Surface analysis

All samples were kept in ambient air after exposure, and the impact of AO exposure on the materials was investigated using several surface analysis techniques, including etch depth measurements, surface chemistry analysis via XPS, and morphology measurements via SEM.

Etch depths were measured by a DekTak surface profiler from Veeco Instruments Inc. Forty steps were measured at different positions for each sample in order to obtain an average etch depth and standard deviation. XPS analysis was conducted before and after exposure with AO fluence $6.31\times10^{20}$ atom/cm$^2$ using a Physical Electronics 5600 located at Montana State University. Surface morphology was obtained before and after exposure to AO fluence of $5.46\times10^{20}$ and $6.31\times10^{20}$ atom/cm$^2$, using a Zeiss SUPRA 55 VP SEM. Before SEM measurement, samples were coated with ∼10 nm thick gold and attached to an aluminum plate using double-sided carbon tape.

## III. RESULTS

### A. Etch depth and erosion yield

Kapton-H is a commonly used polymer for spacecraft. It can be severely eroded by AO and has a erosion yield of $3.0\times10^{-24}$ cm$^3$/atom [1]. So the Kapton-H was chosen as the standard material to estimate the AO fluence and as a comparative criterion to evaluate the AO resistance of other materials. Three AO exposures were carried out in this research. The corresponding AO fluence was derived from the average etch depths of Kapton-H reference samples based on its known erosion yield according to the equation [30]:

$$h = \sigma F \tag{1}$$

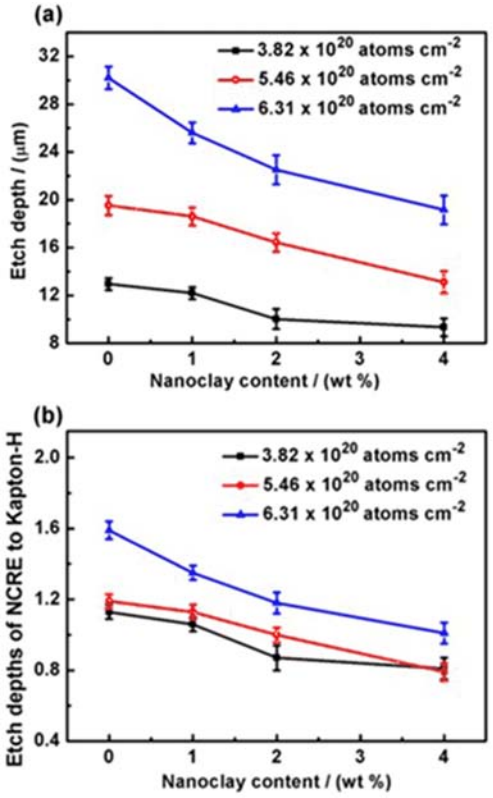


FIG. 3 (a) Etch depths and (b) etch depth ratios of NCRE composites to Kapton-H versus nanoclay contents for AO exposures at three AO fluence: $3.82\times10^{20}$ (black), $5.46\times10^{20}$ (red), and $6.31\times10^{20}$ atom/cm$^2$ (blue).

where $h$, $\sigma$, and $F$ correspond to etch depth, erosion yield, and fluence, respectively. At the studied three AO exposure experiments, the average etch depths of Kapton-H reference samples were (11.45±0.22), (16.39±0.42), and (18.92±0.25) μm, respectively. By substituting the etch depths data and the known erosion yield of Kapton-H into Eq.(1), we can get the AO fluence for the three AO exposures of $3.82\times10^{20}$, $5.46\times10^{20}$, and $6.31\times10^{20}$ atom/cm$^2$, respectively.

Etch depths of pure epoxy and NCRE composites and corresponding etch depth ratios of them to Kapton-H reference sample were obtained and shown in FIG. 3. For all three AO exposures, an increase in nanoclay content was correlated with a decrease in average etch depth and increase in standard deviation of the etch depth measurements (FIG. 3(a)). An increase in standard deviation of the etch depth measurements was also observed in samples exposed to higher AO fluence. The ratio of pure epoxy and NCRE composites to Kapton-H etch depths decreased as nanoclay content increased (FIG. 3(b)). But the lowest ratio was still above 80%, indicating that the etch depth of NCRE composites was relatively high.

Etch depth of NCRE composites was also converted to erosion yield according to Eq.(1). By sub-

DOI:10.1063/1674-0068/cjcp1906119 

TABLE I The relative atomic concentrations of control and exposed NCRE composites with an AO fluence of $6.31\times10^{20}$ atom/cm$^2$.

| Composites | Element in control sample/% | | | | | | Element in exposed sample/% | | | | | |
|---|---|---|---|---|---|---|---|---|---|---|---|---|
| | C 1s | O 1s | N 1s | Si 2p | Al 2p | Others | C 1s | O 1s | N 1s | Si 2p | Al 2p | others |
| Pure epoxy | 79.4 | 13.4 | 2.2 | 2.5 | 0.3 | 2.2 | 71.1 | 20.5 | 4.8 | 0.4 | 0.7 | 2.5 |
| 1 wt% NC | 82.5 | 11.5 | 2.6 | 1.2 | 0.2 | 2.0 | 62.5 | 27.7 | 4.6 | 2.6 | 1.0 | 1.6 |
| 2 wt% NC | 79.5 | 13.1 | 2.3 | 3.1 | 0.1 | 1.9 | 51.5 | 33.7 | 3.9 | 5.4 | 2.1 | 3.4 |
| 4 wt% NC | 70.7 | 17.6 | 2.4 | 6.7 | 0.3 | 2.3 | 42.6 | 39.9 | 3.5 | 7.8 | 2.6 | 3.6 |

stituting the etch depth value and the corresponding AO fluence into Eq.(1), the average erosion yields of pure epoxy and NCRE composites with nanoclay contents of 1 wt%, 2 wt%, and 4 wt% were obtained to be $(3.92\pm0.76)\times10^{-24}$, $(3.55\pm0.45)\times10^{-24}$, $(3.07\pm0.47)\times10^{-24}$, and $(2.63\pm0.35)\times10^{-24}$ cm$^3$/atom respectively.

### B. Surface chemistry

Surface chemistry was investigated using XPS for all samples before and after AO exposure. First, XPS survey scans were conducted to get a comprehensive picture of all elements and their atomic concentrations on the surfaces. Then high resolution XPS spectra of C 1s were collected to obtain further information on chemical bonding.

For both control and exposed samples, the main elemental constituents of epoxy and NCRE composites were identified based on their corresponding principal photoelectron peaks: carbon (C 1s, 284.6 eV), oxygen (O 1s, 533 eV), nitrogen (N 1s, 400 eV), silicon (Si 2p, 103 eV) and aluminum (Al 2p, 76 eV). Besides, trace components from calcium (Ca 2p, 345.9 eV), fluorine (F 1s, 685.7 eV), sodium (Na 1s, 1072.0 eV), and tin (Sn 3d5, 495 eV), were also detected for all the samples. But the atomic concentrations of these elements were quite low and would not affect the whole picture of this research.

Table I presents the relative atomic concentrations of pure epoxy and NCRE composites before and after hyperthermal AO exposure to a fluence of $6.31\times10^{20}$ atom/cm$^2$. It can be seen that for all the samples tested, there is a dramatic change in the surface composition. The most obvious change occurred in carbon and oxygen. The atomic concentrations of C decreased after exposure, accompanied by increase in the atomic concentrations of O. More specifically, atomic concentrations of C decreased by 8.3% (79.4% to 71.1%), 20.0% (82.5% to 62.5%), 28.0% (79.5% to 51.5%), and 28.1% (70.7% to 42.6%) corresponding to pure epoxy, 1 wt%, 2 wt%, and 4 wt% NCRE composites respectively. On the contrary, the increases in O were 7.1% (13.4% to 20.5%), 16.2% (11.5% to 27.7%), 20.6% (13.1% to 33.7%), and 22.3% (17.6% to 39.9%) correspondingly. The decrease in the carbon atomic concentration was more dramatic for the 2 wt% and 4 wt% NCRE composite samples. Likewise, the increase in oxygen atomic concentration was also more dramatic for the nanoclay containing samples than for the pure epoxy samples. An increase in N was also observed as a result of AO bombardment for all the test samples, which was also observed by Awaja *et al.* [13]. Silicon and aluminum atom concentration also displayed an increase after AO exposure for NCRE composites.

High-resolution C 1s XPS spectra of control and exposed samples (FIG. 4) were acquired and show that after AO exposure, all spectra broadened mainly to the high binding energy direction which suggests that the surface was oxidized. The binding energies with peaks at 284.5 eV (peak 1), 286.01 eV (peak 2), 288 eV (peak 3), 282.48 eV (peak 4) were attributed to C−C/C−H, C−O, ketones, and carbides respectively. Furthermore, following AO exposure for the nanoclay containing samples, a new peak arose at 290.87 eV in the spectra (labeled as peak 5 in FIG. 4(b)) and was attributed to carbonates. An analysis of the relative area of C-related bonds from the high-resolution C 1s XPS spectra in FIG. 4 before and after AO exposure (Table II) shows that decrease in overall carbon atomic concentration is accompanied by the increase of oxygen-containing carbon species C−O, ketones, and carbonates, and decrease of C−C/C−H, indicating that all samples were eroded and oxidized by hyperthermal AO. In more detail, for pure epoxy, 1 wt%, 2 wt%, and 4 wt% NCRE composites, the decreases of C−C/C−H component are 34.1% (86.3% to 52.2%), 29.6% (78.4% to 48.8%), 33.9% (80.6% to 46.7%), and 37.2% (78.1% to 40.9%), the increases of C−O component are 32.3% (6.9% to 39.2%), 32.5% (8.0% to 40.5%), 25.1% (5.7% to 30.8%), and 19.1% (17.2% to 36.3%), the increases of ketone component are 2.5% (2.7% to 5.2%), 2.0% (2.9% to 4.9%), 6.3% (3.5% to 9.8%), and 9.2% (1.8% to 11.0%), the increases of carbonates are 0%, 1.6%, 3.5%, and 3.7%, the sums of the increase of oxygen-relating C component are 34.8%, 36.1%, 34.9%, and 32.0%, respectively.

### C. Surface morphology

Surface morphologies of control and samples exposed to AO fluence of $5.46\times10^{20}$ and $6.31\times10^{20}$ atom/cm$^2$ are shown in FIG. 5 and FIG. 6. From low-

DOI:10.1063/1674-0068/cjcp1906119 

TABLE II Relative area proportions of carbon species of control and exposed samples with an AO fluence of $6.31\times10^{20}$ atom/cm$^2$.

| Composites | Area proportions in control sample/% | | | | Area proportions in exposed sample/% | | | | |
|---|---|---|---|---|---|---|---|---|---|
| | C−C/C−H | C−O | Ketones | Carbides | C−C/C−H | C−O | Ketones | Carbides | Carbonates |
| Pure epoxy | 86.3 | 6.9 | 2.7 | 4.1 | 52.2 | 39.2 | 5.2 | 3.3 | - |
| 1 wt% NCRE | 78.4 | 8.0 | 2.9 | 9.2 | 48.8 | 40.5 | 4.9 | 4.2 | 1.6 |
| 2 wt% NCRE | 80.6 | 5.7 | 3.5 | 9.4 | 46.7 | 30.8 | 9.8 | 9.2 | 3.5 |
| 4 wt% NCRE | 78.1 | 17.2 | 1.8 | 2.4 | 40.9 | 36.3 | 11.0 | 8.1 | 3.7 |

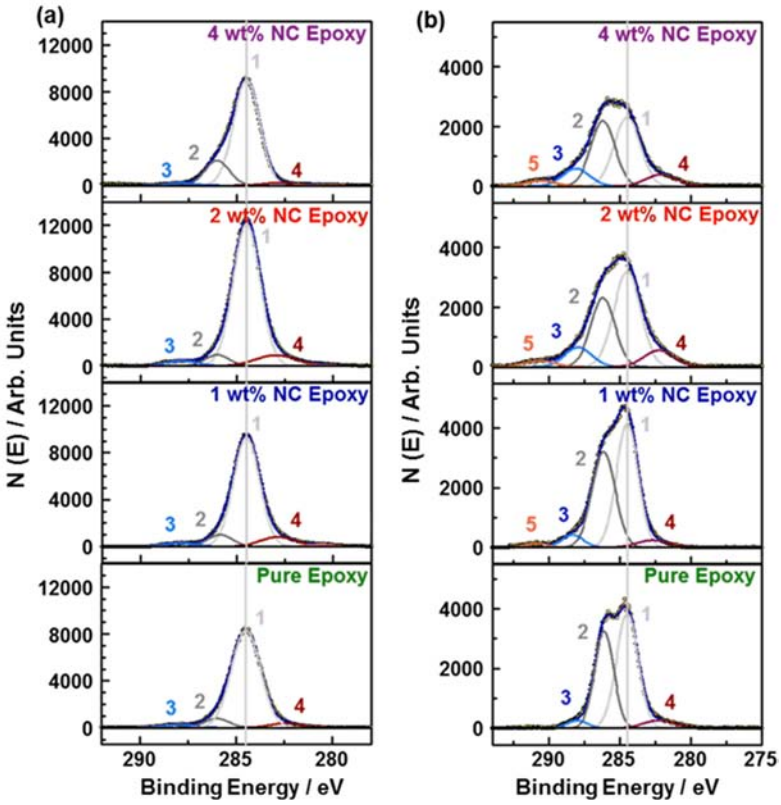


FIG. 4 High-resolution C 1s spectra of (a) control and (b) exposed samples with an AO fluence of $6.31\times10^{20}$ atom/cm$^2$.

magnification SEM images in FIG. 5, the control pure epoxy sample surface exhibited an egg-crate-like wrinkled pattern. Besides this egg-crate-like wrinkled pattern, the control NCRE composites also showed high-contrast nanoclay clusters on the surface. After exposure to AO fluence of $5.46\times10^{20}$ and $6.31\times10^{20}$ atom/cm$^2$, the pure epoxy samples revealed distributed erosion pits. NCRE samples revealed aggregates of different sizes. The distribution densities of the aggregates increased with increasing nanoclay content and AO fluence. In more detail, three aspects of SEM images results are worth noting. Firstly, as the mixing of nanoclay, NCRE composites presented a diverse surface morphology compared to pure epoxy after exposure to AO beam. Secondly, longer exposure (higher AO fluence) caused rougher surface than shorter exposure (lower AO fluence). After an exposure of $6.31\times10^{20}$ atom/cm$^2$, all the NCRE composites had a rougher surface morphology than samples exposed to $5.46\times10^{20}$ atom/cm$^2$. Lastly, the surface roughness was related to the nanoclay content. NCRE composite with higher content of nanoclay was apparently much rougher than the lower content nanoclay of NCRE composite for a given fluence exposure.

High-magnification SEM images (FIG. 6) show that the roughness of the control NCRE samples increases with increasing nanoclay content. Following AO exposure, the pure epoxy sample surfaces were relatively smooth with some etch pits forming. These etch pits were distributed on the surface randomly. Like the low magnification SEM images results, as the nanoclay content increased, aggregates were observed on the sample surfaces. In addition, following the increasing fluence of AO exposure, more and more aggregates formed on

DOI:10.1063/1674-0068/cjcp1906119 

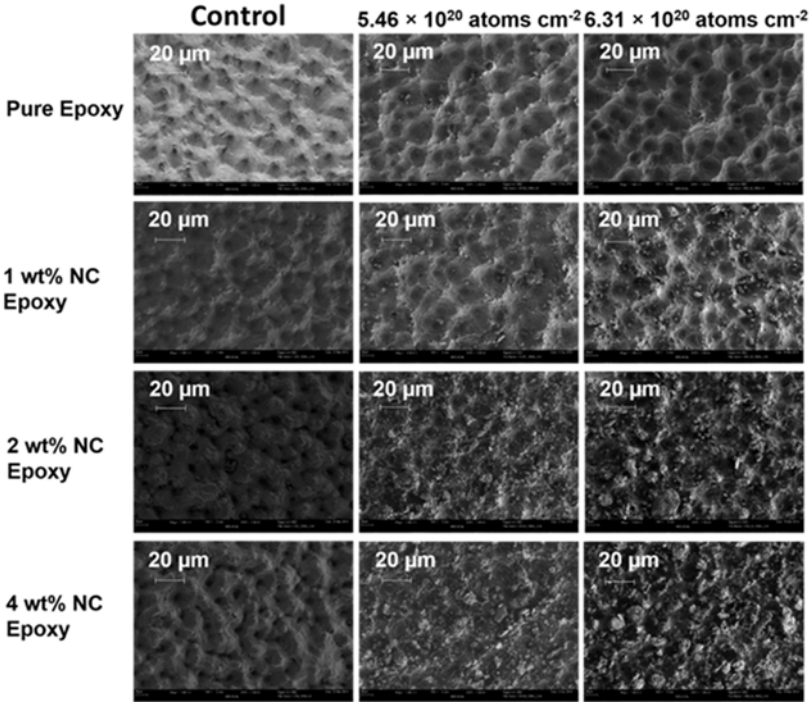


FIG. 5 From top to bottom: low-magnification SEM images of pure epoxy, 1 wt%, 2 wt%, and 4 wt% nanoclay reinforced epoxy. From left to right: low-magnification SEM images of control samples, exposed samples with AO fluence of $5.46\times10^{20}$ and $6.31\times10^{20}$ atom/cm$^2$.

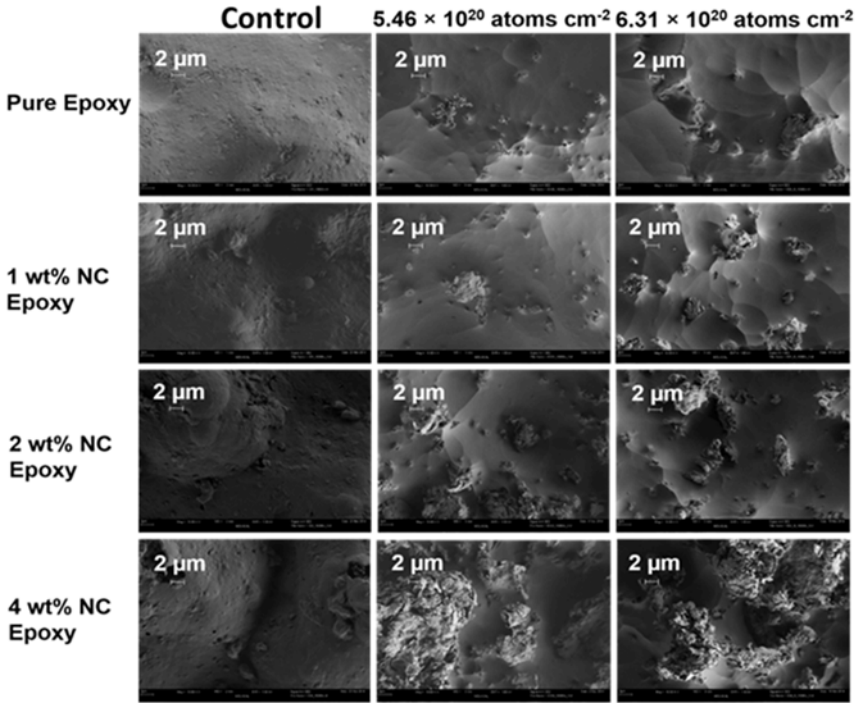


FIG. 6 From top to bottom: high-magnification SEM images of pure epoxy, 1 wt%, 2 wt%, and 4 wt% nanoclay reinforced epoxy. From left to right: high-magnification SEM images of control samples, exposed samples with AO fluence of $5.46\times10^{20}$ and $6.31\times10^{20}$ atom/cm$^2$.

DOI:10.1063/1674-0068/cjcp1906119 

the NCRE samples surface and these aggregates were more exposed with longer exposure. Furthermore, it is obviously from these high magnification SEM images that the size of aggregates increased as the increasing nanoclay content and increasing AO fluence.

## IV. DISCUSSION

In this study, etch depth was observed for both pure epoxy and nanoclay containing NCRE composites after exposure to AO, which indicates that both pure epoxy and nanoclay reinforced epoxy samples were etched during exposure to hyperthermal AO attack. During exposure, AO attacked the surface and eroded samples by releasing volatile products, which resulted in the etch depth. Pure epoxy did not show favorable AO resistance when compared to the Kapton-H reference. Etch depth ratios of pure epoxy to Kapton-H of three exposures increased from 1.13, 1.19, to 1.60, with increasing AO fluence. This can also be seen from the calculated average erosion yield of pure epoxy $(3.92\pm0.76)\times10^{-24}$ $cm^3$/atom. In contrast, NCRE composites exhibited lower etch depths. A clear trend was observed of decreasing average etch depths of NCRE composites with increasing content of nanoclay reinforcement, which indicates that AO resistance of epoxy was bolstered by nanoclay reinforcement. The 4 wt% NCRE composite, with the largest content of nanoclay in this study, showed the highest resistance to AO with etch depths ranging from 28% to 37% compared to pure epoxy samples after exposure to the three AO fluence studied. Of all the samples tested, 4 wt% NCRE composite exhibited the lowest average erosion yield of $(2.63\pm0.35)\times10^{-24}$ $cm^3$/atom, which dropped down significantly in comparison with pure epoxy. Given that the nanoclay mainly contains O, Si, and Al, and nanoclay reacts with epoxy to form a chemical bond [17], the NCRE samples are expected to have lower erosion depths and erosion yields. Indeed, the SEM results show that the nanoclay clusters become more and more exposed with increasing AO fluence, indicating that the nanoclay clusters etch at a slower rate than the epoxy resin. Apparently, nanoclay clusters impeded AO attack of epoxy resin and reduced the erosion depth and erosion yield. For the largest content of nanoclay in this study, the NCRE composite reached the lowest erosion depth and erosion yield. Unfortunately, in current study we can not give a detailed understanding of reaction mechanism on how the nanoclay impede the chemical reactions which carry mass away and cause erosion depth.

Variations in etch depth became more apparent with increasing content of nanoclay reinforcement and AO fluence, indicating increased surface roughness, which commensurate with SEM images. The decreased etch depth and increased surface roughness reveal that NCRE composites experienced milder erosion, with less mass taken away by volatile reaction products and relatively more non-volatile oxidized products staying on the surface.

XPS information reveals chemical changes on surfaces and provides insight into reaction mechanism of pure epoxy and NCRE composites with AO. The changes in surface element concentrations show that for all the samples atomic concentration of C decreased while that of O increased after AO exposure, indicating that sample surfaces were eroded and oxidized, which has also been observed in previous studies on polymers exposed to AO [11, 13, 31, 32]. This is because of the high energy and the strong oxidizing property of the hyperthermal AO. Energetic collisions of hyperthermal AO with sample surfaces can degrade materials by erosion and oxidation reaction, through breaking weak bonds and creating new chemical bonds. During hyperthermal AO bombardment, volatile molecules CO, $CO_2$ and OH would be produced and carry mass away from polymer surface, which has been demonstrated in previous studies [33]. This is called erosion process [34]. Due to erosion, the remaining surface will be roughened and etch depth will be formed. Besides the erosion process, reaction between high energy O atoms and sample surfaces can also produce non-volatile products left on the surfaces and make surfaces oxidized, which is called oxidation process [34]. Given that pure epoxy and NCRE composites are all mainly composed of carbon elements with C−C/C−H bond, it is reasonable that during bombardment of AO, C−C/C−H bond was broken and volatile products CO, $CO_2$ and OH were produced and flew off the surface. Since these products contain surface carbon and hydrogen atoms, these products must account for the majority of the erosion depth and the decrease of atomic concentration of C shown in Table I. Since the formation of these products involves breakage of C−C/C−H bonds, this erosion process must contribute to the decrease of relative area of C−C/C−H component shown in FIG. 4 of exposed samples when comparing to control samples. In addition to the old chemical bonds breakage, new chemical bonds were also created and non-volatile products stayed (like C−O, ketones, carbonates, *etc.*) on surfaces. This oxidation process contributes to the increase of atomic concentration of O shown in Table I and increase of relative area of C−O, ketones, and carbonates peaks shown in FIG. 4. Although all the samples were eroded and oxidized by hyperthermal AO, for the exposed samples, the pure epoxy showed the highest C concentration (71.1%), while 4 wt% NCRE composite showed the lowest C concentration (42.6%). This is in contrary to the expectation from the results by Firas *et al.* [13]. This seems to be accounted for mainly in the lowest O concentration (20.1%) on pure epoxy and the highest O concentration (39.9%) on 4 wt% NCRE composite. We speculate that the highest O concentration on 4 wt% NCRE composite might be the result of that more O-related products were non-volatile than on

DOI:10.1063/1674-0068/cjcp1906119 

pure epoxy, 1 wt%, and 2 wt% composites.

The increase in N concentration after AO exposure is consistent with surface erosion and was particularly believed to be more redistribution of eroded material at the surface [13]. The increase in Si and Al atom concentration after AO bombardment is the result of that during exposure more Si and Al in nanoclay clusters were exposed on surfaces. High resolution spectra of C 1s indicated that, as the samples were exposed, carbon species were gradually oxidized, which resulted in a broadening of C peak and occurrence of a new peak (peak 5, FIG. 4(b)) of carbonates near 290.7 eV. The broadened carbon peak was resulted from the decrease in C−C bonds and concomitant increase in C−O bonds, ketones, and carbonates. It appears that the surface oxidation extent got increased for both pure epoxy and NCRE composites by reaction with hyperthermal AO. This is due to that components C−C/C−H with low binding energy are susceptible to the formation of C−O, ketones and carbonates components with high binding energy through breaking of C−C/C−H bonds by hyperthermal atomic oxygen. Specifically, pure epoxy exhibited most C−O component increase, while 4 wt% NCRE composite exhibited most ketones and carbonates increase. Furthermore, nanoclay containing composites favors the formation of the new component carbonates. It appears that addition of nanoclay makes the reaction between surface and energetic AO more prone to produce high oxide components (ketone, carbonates). This is probably related to the interfacial bonding formed between nanoclay and epoxy [17]. From the total increase in oxygen-relating C component, it can be seen that 4 wt% NCRE component got least oxidized, consistent with the smallest erosion depth. Although pure epoxy, 1 wt% NCRE, and 2 wt% NCRE showed similar oxidation extent, it is probably because of the different erosion extent that caused the different erosion depths. Unfortunately, current study does not permit a more detailed understanding of the reaction mechanism through which how nanoclay act to enhance the AO resistance of epoxy.

Surface morphology changed significantly after AO exposure, as can be seen in FIG. 5 and FIG. 6. The surface morphology of exposed samples was the combined results of oxidation and erosion caused by hyperthermal AO [34]. Compared with control sample, except the erosion pits, the exposed pure epoxy showed a smoother surface morphology, which can be seen obviously in high-magnification SEM images. From the surface morphology evolution of pure epoxy, it can be deduced that the reaction between hyperthermal AO and pure epoxy was mainly erosion. As a comparison, the NCRE samples showed a different surface morphology evolution process with the increase of AO fluence. Due to erosion, epoxy part of the NCRE samples showed relative smooth surface morphology. Besides that, nanoclay clusters evolved to aggregates, which were clearly seen on the surface of NCRE samples. The size and distribution densities of the aggregates increased with the increasing nanoclay content and AO fluence, which lead to the observed increase in surface roughness in SEM images. Evidently, the reaction between hyperthermal AO and NCRE samples was more complex than that with pure epoxy. The exposed NCRE samples appear to be visibly covered with aggregations after AO exposure. The produced aggregates potentially act as a "physical shield" and protected epoxy below from being attacked by hyperthermal AO. Unfortunately, no direct correlation was found between surface morphologies and changes in surface chemistry. The aggregation layers were imperfect as gaps formed in areas where epoxy unprotected by the nanoclay was eroded by AO (FIG. 6). Therefore, compared to reference Kapton-H samples, the 4 wt% NCRE samples still showed significant erosion and consequently relatively high etch depth ratios to Kapton-H.

## V. CONCLUSION

Epoxy resin composites with different content of nanoclay reinforcement have been evaluated under ground simulated LEO atomic oxygen conditions by use of laser detonation AO source. The addition of nanoclay enhanced the resistance of NCRE composites to AO attack through reduced erosion depth. Occurrence of chemical reactions such as erosion and oxidation resulting from degradation by the AO was apparent from XPS data of all the tested samples. The degree of surface oxidation was related to the nanoclay weight percentage. The 4 wt% NCRE composite suffered least surface oxidation after AO bombardment. Erosion feature was observed in surface morphology of both pure epoxy and NCRE composites. Nanoclay clusters etched at a slower rate than the epoxy resin and the produced aggregates occurred on NCRE composite surfaces. The aggregates potentially act as a "physical shield" and partly protect epoxy below from being attacked by hyperthermal AO.

## VI. ACKNOWLEDGMENTS

This work was supported by the National Natural Science Foundation of China (No.21473015 and No.41574101), and the Fundamental Research Funds for the Central Universities (No.3132018233).

[1] R. C. Tennyson, Can. J. Phys. **69**, 1190 (1991).
[2] E. Murad, J. Spacecraft Rockets **33**, 131 (1996).
[3] M. R. Reddy, J. Mater. Sci. **30**, 281 (1995).
[4] S. Packirisamy, D. Schwam, and M. H. Litt, J. Mater. Sci. **30**, 308 (1995).
[5] E. Grossman and I. Gouzman, Nucl. Instrum. Meth. B **208**, 48 (2003).

DOI:10.1063/1674-0068/cjcp1906119 

[6] T. K. Minton, B. H. Wu, J. M. Zhang, N. F. Lindholm, A. I. Abdulagatov, J. O'Patchen, S. M. George, and M. D. Groner. ACS Appl. Mater. Inter. **2**, 2515 (2010).
[7] G. S. Arnold and D. R. Pehlinski, AIAA J. **23**, 976 (1985).
[8] G. S. Arnold and D. R. Peplinski, AIAA J. **23**, 1621 (1985).
[9] R. Cooper, H. P. Upadhyaya, T. K. Minton, M. R. Berman, X. Du, and S. M. George, Thin Solid Films **516**, 4036 (2008).
[10] I. Gouzman, O. Girshevitz, E. Grossman, N. Eliaz, and C. N. Sukenik, ACS Appl. Mater. Inter. **2**, 1835 (2010).
[11] R. Verker, E. Grossman, I. Gouzman, and N. Eliaz, High Perform. Polym. **20**, 475 (2008).
[12] T. K. Minton, M. E. Wright, S. J. Tomczak, S. A. Marquez, L. Shen, A. L. Brunsvold, R. Cooper, J. Zhang, V. Vij, A. J. Guenthner, and B. J. Petteys, ACS Appl. Mater. Inter. **4**, 492 (2012).
[13] F. Awaja, J. B. Moon, M. Gilbert, S. Zhang, C. G. Kim, and P. J. Pigram, Polym. Degrad. Stabil. **96**, 1301 (2011).
[14] A. Jumahat, C. Soutis, F. R. Jones, and A. Hodzic, Plast. Rubber Compos. **41**, 225 (2012).
[15] M. L. Chan, K. T. Lau, T. T. Wong, M. P. Ho, and D. Hui, Compos. Part B-Eng. **42**, 1708 (2011).
[16] K. Lau, M. Lu, J. Qi, D. Zhao, H. Cheung, C. Lam, and H. Li, Compos. Sci. Technol. **66**, 450 (2006).
[17] M. L. Chan, K. T. Lau, T. T. Wong, and F. Cardona, Appl. Surf. Sci. **258**, 860 (2011).
[18] M. W. Ho, C. K. Lam, K. T. Lau, D. H. L. Ng, and D. Hui, Compos. Struct. **75**, 415 (2006).
[19] C. K. Lam, H. Y. Cheung, K. T. Lau, L. M. Zhou, M. W. Ho, and D. Hui, Compos. Part B-Eng. **36**, 263 (2005).
[20] H. L. Ma, X. Zhang, K. T. Lau, and S. Q. Shi, J. Compos. Mater. **52**, 2477 (2017).
[21] A. A. Azeez, K. Y. Rhee, S. J. Park, and D. Hui, Compos. Part B-Eng. **45**, 308 (2013).
[22] H. Fong, R. A. Vaia, J. H. Sanders, D. Lincoln, A. J. Vreugdenhil, W. Liu, J. Bultman, and C. Chen, Chem. Mater. **13**, 4123 (2001).
[23] C. K. Lam and K. T. Lau, Mater. Lett. **61**, 3863 (2007).
[24] Y. Sugita, C. Winkelmann, and V. La Saponara, Compos. Sci. Technol. **70**, 829 (2010).
[25] A. Toldy, B. Szolnoki, and G. Marosi, Polym. Degrad. Stabil. **96**, 371 (2011).
[26] L. Guadagno, M. Raimondo, V. Vittoria, L. Vertuccio, C. Naddeo, S. Russo, B. D. Vivo, P. Lamberti, G. Spinelli, and V. Tucci, RSC Adv. **4**, 15474 (2014).
[27] S. Yagnamurthy, Q. Chen, C. Chen, and I. Chasiotis, J. Compos. Mater. **47**, 107 (2012).
[28] D. M. Buczala, A. L. Brunsvold, and T. K. Minton, J. Spacecraft Rockets **43**, 421 (2006).
[29] G. E. Caledonia, R. H. Krech, and B. D. Green, AIAA J. **25**, 59 (1987).
[30] X. Wang, X. Zhao, M. Wang, and Z. Shen, Polym. Eng. Sci. **47**, 1156 (2007).
[31] G. Bitetti, M. Marchetti, S. Mileti, F. Valente, and S. Scaglione, Acta Astronaut. **60**, 166 (2007).
[32] F. Awaja, J. B. Moon, S. Zhang, M. Gilbert, C. G. Kim, and P. J. Pigram, Polym. Degrad. Stabil. **95**, 987 (2010).
[33] H. Wang, M. Qian, V. J. Murray, B. Wu, Y. Yang, A. Dong, L. Che, and T. K. Minton, High Perform. Polym. **31**, 472 (2018).
[34] T. K. Minton and D. J. Garton, *Chemical Dynamics in Extreme Environment*, R. A. Dressler Ed., Singapore: World Scientific, 420 (2001).

DOI:10.1063/1674-0068/cjcp1906119 